Mixed correlation phases in elongated quantum dots

A. Ballester,[1] J. M. Escartín,[2] J. L. Movilla,[1] M. Pi,[2] and J. Planelles[1,*]
[1]*Departament de Química Física i Analítica, Universitat Jaume I, P.O. Box 224, E-12080 Castelló, Spain*
[2]*Departament ECM, Facultat de Física, IN2UB, Universitat de Barcelona, E-08028 Barcelona, Spain*
(Received 13 May 2010; published 7 September 2010)

It is theoretically shown, within the local spin-density-functional theory framework, that inhomogeneous confining potentials in elongated, diluted *N*-electron quantum dots may lead to the formation of mixed phases in which some regions of the *N*-electron system behave like a Fermi liquid while, simultaneously, other, more dilute regions display quasiclassical Wigner crystallization. The characterization of the mixed phases in the addition energy spectrum and the infrared response is reported. An infrared sensor of electron filling is suggested.

DOI: 10.1103/PhysRevB.82.115405 PACS number(s): 73.21.−b, 71.15.Mb, 73.22.Gk, 85.35.Be

I. INTRODUCTION

In 1934 Wigner[1] predicted that, below a critical electron density, the electron gas crystallizes and forms a lattice of electrons arranged in precise classical configurations. This is due to the fact that the kinetic energy becomes negligible relative to the Coulomb energy so that correlations dominate the electronic structure. Many classical electron configurations in quantum dots (QDs) have been reported up to date (see, e.g., Refs. 2 and 3), and classical rotational and vibrational models have shown quantitative agreement with quantum-mechanical treatments.[4,5] All the same, Wigner crystals in QDs do not actually consist of classical pointlike electrons but of quantum electrons having finite extension, which is of relevance for the properties of these crystals. It should be mentioned that, in addition to their intrinsic theoretical interest, these strongly correlated states are of technological significance, e.g., because of their potential use in nanoscale systems for the implementation of qubits and quantum logic gates in quantum computers.[6]

Many studies show that the quantum melting proceeds through intermediate, partially melted Wigner molecular states. Quantum melting is the transition from an ordered strongly correlated Wigner crystal to a Fermi liquid, i.e., to a system of weakly interacting particles where the kinetic energy dominates the Coulomb repulsion. This melting is induced by an increase in the confining potential strength. Thus, in the case of *N* electrons confined in a 2D parabolic trap, we first face an angular melting, yielding a radially ordered crystal, and a further radial melting finally yields the Fermi liquid.[7–9] Similar behavior is observed in a three-particle Wigner molecule confined in a 2D torus, the melting of which proceeds through an intermediate state that can be described as a delocalized electron plus a rigid two-particle Wigner molecule.[10] In the case of *N*-electron quasi-one-dimensional systems, the Wigner phase is characterized by a density profile with *N* peaks regularly spaced along the axial direction. The transition to the Fermi liquid goes through an intermediate phase, called charge-density wave (CDW),with $N/2$ peaks in the density profile.[2,11–13] This phase may also be considered as a partially melted Wigner molecule.

In contrast, crystallization processes in the presence of highly inhomogeneous potentials seem to have attracted much less attention. On the one hand, Wigner crystallization in the presence of an attractive defect was considered, albeit briefly, by Szafran *et al.*[14] They studied a quasi-one-dimensional QD populated with $N=2$ and $N=3$ electrons and perturbed by a steplike defect potential localized at the center of the system. In the absence of the defect, their configuration-interaction (CI) study reveals that the number of maxima equals the number *N* of electrons, as corresponds to Wigner molecules. After switching on the defect, three charge maxima in the electron-density profile arise in both cases. They conclude then that the influence of the central attractive potential showed to be qualitatively different for $N=2$ and $N=3$ electrons. While for the even case the defect potential destroys the Wigner crystallization, yielding an extra maximum, for $N=3$ it simply enhances the localization of the central electron. Also, incidentally, in Fig. 10 of Appendix B in Ref. 15, a representation of the electron densities corresponding to a Hartree-Fock calculation of a strictly one-dimensional box with a double-well-like potential profile is displayed. An interesting feature emerges in this picture, which is only briefly referred to in the figure caption. Namely, the represented state show a low-density crystal-like central region surrounded by a high-density liquidlike one.

In general, Wigner molecules are associated with weak-confinement regimes. However, it has been reported[16] that the presence of the narrow, deep self-polarization potential coming from the dielectric mismatch at the QD border in free standing small spherical two-electron nanocrystals may induce the formation of surface states. These states concentrate the electronic density within the narrow, deep well at the QD surface, i.e., are in the strong-confinement regime and, nevertheless, show an angular Wigner type of localization.[16]

Finally, the effect of the effective electron-mass anisotropy on the Wigner phase formation has also been explored.[17] The study is motivated by the fact that effective electron-mass anisotropy may occur in semiconductor materials. The authors theoretically explore a 2D system and conclude that anisotropic electrons require larger spacing to form Wigner lattices.

In a recent paper,[13] we theoretically studied, within the local spin-density-functional theory (LSDFT), the electronic structure of nanorods (NRs), elongated QDs which constitute the bridge between zero-dimensional QDs and one-

dimensional quantum wires (QWs), and monitorized the Wigner crystallization in the addition energy spectra. Note that, by changing the gate voltage attached to a nanocrystal, tunnel conductance and capacitance measures yield a peak every time the number of electrons in the QD increases by one. The spacing of peaks, or addition spectrum, reflects differences between the ground states with different numbers of electrons and can be used to monitorize localization-delocalization transitions in QDs.[18] Additionally, calculated electron-density profiles nicely displayed the phase transition found in the low-density limit, from CDW, with $N/2$ peaks in the density profile and preserved spin symmetry, to spin-density waves (SDW), with N peaks (Wigner crystallization) and broken spin symmetry.[19] The LSDFT calculation was supported with a few CI calculations. We would like to stress that investigations on the transition regime from QDs to QWs are of particular interest in the case of these colloidal, elongated semiconductor nanocrystrals because size and shape control enables the synthesis of NRs with precise length and diameter[20] so that one can follow the transition from zero- to one-dimensional systems by tuning their aspect ratio.

To the best of our knowledge, except in the above mentioned, strictly one-dimensional Hartree-Fock calculation by Mueller,[15] no new phases produced by perturbing potentials or anisotropic effective masses have been reported to date. In the present paper we will show that inhomogeneous confining potentials may lead to the formation of new phases in truly three-dimensional systems, driven by an uneven electronic-density distribution, in which some regions of the N-electron system behave like a Fermi liquid while, simultaneously, other more dilute regions display the typical quasiclassical Wigner distribution of the charge maxima in the electron-density profile. Hereafter we will refer to these phases as mixed phases (MPs). We will show that one can get a MP by applying an electric field along the longitudinal axis of a dilute NR. Nowadays, though, there is another way to modify the NR confining potential which we will show renders better defined MPs than those produced by an external electric field. It is the chemical synthesis of nanodumbbells (NDs).[21–23] Nanodumbbells are NRs of a given material sandwiched between two-end spherical caps of a different material. Then we first will look for MPs in nanodumbbells, i.e., MPs produced by structural effects. Afterwards, we will study MPs in diluted NRs subject to an electric field along the NR axis. Also, we will pay attention to the way of probing MPs, in particular, the addition spectrum and the infrared response.

II. THEORY AND MODELS

LSDFT, also referred to as local spin-density-approximation (LSDA), which has given satisfactory results in the study of related structures,[12,24–26] is employed in the present work. Numerical integration of the Kohn-Sham (KS) equations is carried out. Details of the method followed are described in Ref. 24. The exchange-correlation functional is taken as a sum of the Dirac exchange functional of a homogeneous electron gas and the correlation-functional parametrized by Perdew and Zunger.[27]

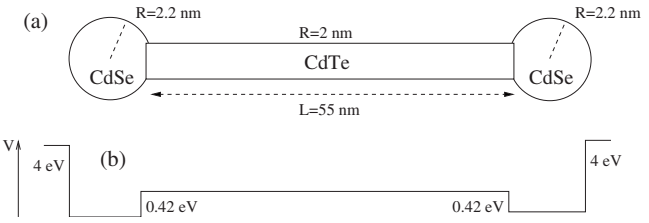

FIG. 1. (a) Schematic geometry of the nanostructures under study. (b) Schematic profile of the spatial confining potential along the z axis.

In addition to the ground-state calculations, we also compute the spin- and charge-density responses within the framework of time-dependent LSDFT.[28] In order to obtain the dipole strength in the spin and density channels, we study the time evolution, following an initial perturbation, of the dipole signal $\mathcal{D}(t)=\mathbf{n}\cdot\langle\mathbf{D}\rangle$, where $\mathbf{D}=\Sigma_j\mathbf{r}_j$ for density-dipole modes and $\mathbf{D}=\Sigma_j\mathbf{r}_j\sigma_j^z$ for spin-dipole modes, $\langle\cdot\rangle$ means expected value in the time-dependent state, and $\mathbf{n}$ is the unit vector pointing toward the direction given by the polarization of the incident electromagnetic wave. To calculate $\mathcal{D}(t)$, we first solve the static LSDA KS equations, and the appropriate static solutions of the KS equations are then used as initial conditions for solving the time-dependent KS equations,

$$i\hbar\frac{\partial}{\partial t}\Psi_\sigma(\mathbf{r},t)=\mathcal{H}_{\mathrm{KS}}[\rho_\uparrow(\mathbf{r},t),\rho_\downarrow(\mathbf{r},t)]\Psi_\sigma(\mathbf{r},t). \quad (1)$$

In order to describe the interaction of the system with an external dipole field, the ground-state single-particle (sp) wave functions are slightly excited initially according to $\Psi'_\sigma(\mathbf{r},0)=U\Psi_\sigma(\mathbf{r},0)$, with $U=\exp(ik\mathbf{n}\cdot\mathbf{r})$ for the density-dipole modes and $U=\exp(ik\eta_\sigma\mathbf{n}\cdot\mathbf{r})$, where $\eta_\sigma=+1(-1)$ for $\sigma=\uparrow(\downarrow)$, for the spin-dipole modes. The wave number k is taken small enough to keep the response of the system within the linear regime, in which the Fourier transform of the dipole signal, $\mathcal{D}(\omega)=\int e^{i\omega t}\mathcal{D}(t)dt$, is directly related to the dipole strength, $S_{\mathbf{n}}(\omega)=\frac{1}{k}\mathrm{Im}[\mathcal{D}(\omega)]$. Hence, a frequency analysis of $\mathcal{D}(t)$ provides the absorption energies and their respective intensities (see details in Refs. 28 and 29).

Unless otherwise stated, we study Wigner crystallization and MPs in CdTe NRs and CdSe/CdTe/CdSe NDs. The NR is modeled by a cylinder of radius $R=2$ nm and length $L=55$ nm, and the ND is built by attaching two $R=2.2$ nm radius spherical caps to this NR, as depicted in Fig. 1. A twofold reason leads us to choose these materials. On the one hand, they are materials employed nowadays in many syntheses of elongated nanocrystals,[21–23] and, on the other hand, they have very similar effective masses and dielectric constants, but they have a rather large band offset so that no relevant effects coming from effective mass and/or dielectric constant inhomogeneities will mask those coming from an inhomogeneous confining potential derived from the band offset. The uniform electron effective mass, $m^*=0.13$, and dielectric constant, $\epsilon=9.2$, employed in our models are those of bulk material.[30] We assume the 0.42 eV CdSe/CdTe conduction-band offset[31] as confining barrier height between

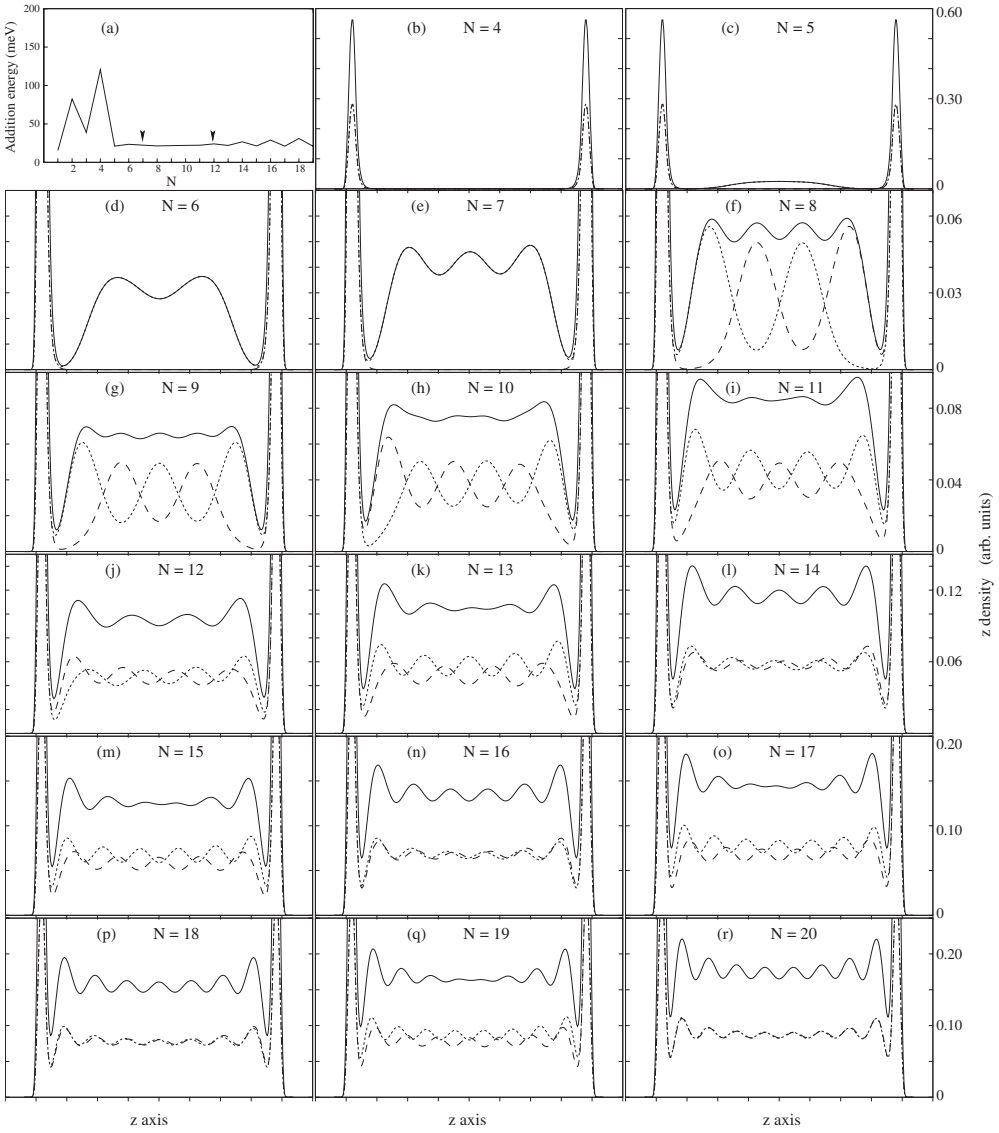

FIG. 2. (a) Addition energy spectrum of the studied nanodumbbell (cylinder of $R=2$ nm radius and length $L=55$ nm, ended with two $R=2.2$ nm radius spherical caps). [(b)–(r)] Ground state z-density profiles of this nanodumbbell populated with 4 up to 20 electrons, respectively. Solid line: total charge density. Dotted/dashed line: spin up/down density. Panels (d)–(r): density profiles have been cut to better display it in the ND trunk region.

these materials. Since no specific QD environment is determined, we assume a typical 4 eV confining QD-environment barrier (see Fig. 1).

III. RESULTS AND DISCUSSION

We first study the electronic structure of CdSe/CdTe/CdSe NDs. The geometry, material parameters, and confining potential are those described in the previous section. The geometry has been selected to show the gradual appearance of the different phases.

In Fig. 2(a) we show the addition energy spectrum of this ND, i.e., the energy $E_{\mathrm{add}}(N)=U(N+1)-2U(N)+U(N-1)$, where $U(N)$ is the total energy of the N-electron system ground state. As stated in Sec. I, this magnitude, analogous to the electron affinity in atomic physics, quantifies the relative stability of the N-particle system and can be measured experimentally as a function of N. It constitutes a key quantity that characterizes transport into the nanostructures.

In order to theoretically obtain this spectrum, the more rigorous, but computationally very demanding, exact diagonalization could be attempted. In practice, unfortunately, this heavy method can only be applied to few-electron systems. Larger systems require less-demanding methods, such as the DFT here employed. The practical limitations of this method come from the not exactly known exchange-correlation potential but general experience is that DFT results are quite reliable,[32] and they have substantially contributed to an understanding of QD addition spectra.[2,33]

The addition energy profile, see Fig. 2(a), shows a peak at $N=2$ electrons corresponding to a half filling of the first $\ell_z=0$ shell, and a second, larger peak at $N=4$ electrons, corresponding to the complete filling of this shell. Up to $N=4$

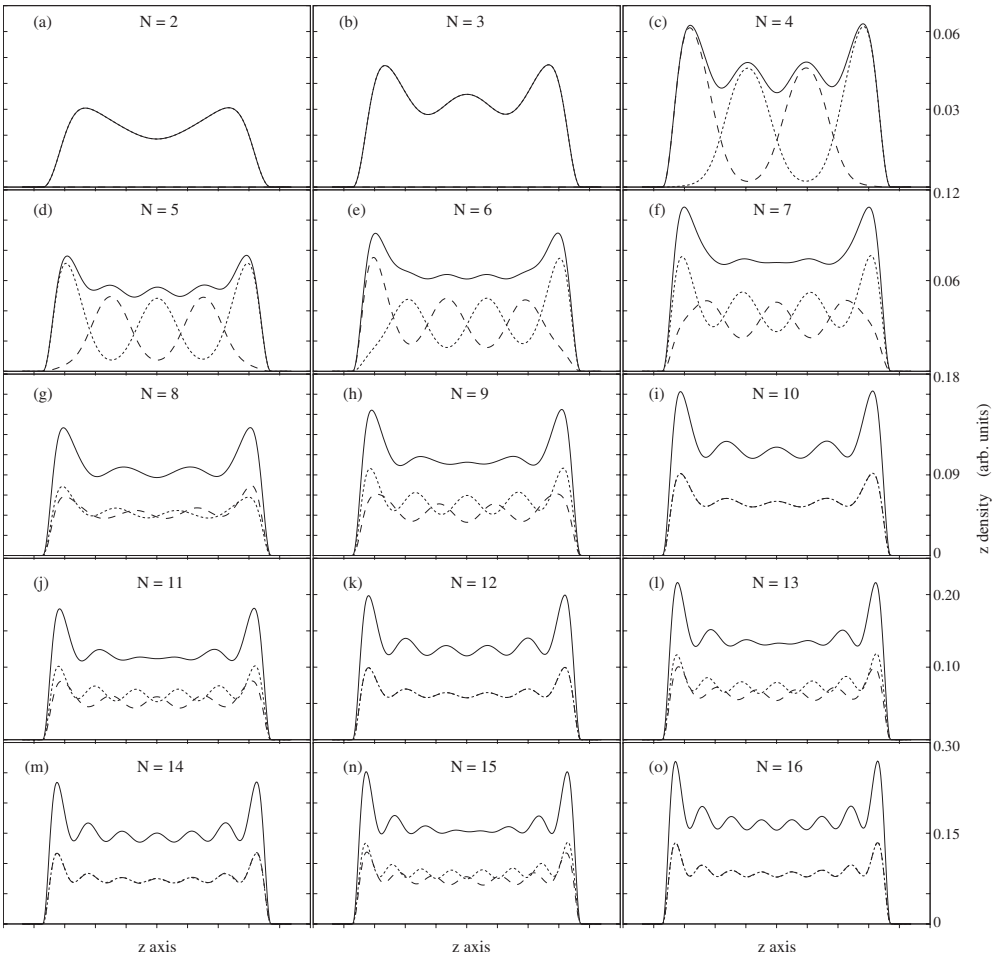

FIG. 3. Ground state z-density profiles of the studied nanorod (cylinder of $R=2$ nm radius and length $L=55$ nm) populated with 2 up to 16 electrons, respectively. Solid line: total charge density. Dotted/dashed line: spin up/down density.

electrons the density is completely localized within the ND spherical caps, as can be seen in Fig. 2(b), where the ground-state z-density profile, i.e., $\rho(z)=\int\rho(r,z,\phi)dS$, of the ND populated with $N=4$ electrons is represented. As can be seen, for $N=4$, the electronic spin-up density (dotted line) equals the electronic spin-down density (dashed line), adding up to the total density [solid line in Fig. 2(b)].

After filling the ND with $N=4$ electrons, the addition energy profile shows a flat region. It corresponds to the filling of sp wave functions localized in the ND cylinder. Thus, Fig. 2(c) shows how the fifth electron with spin up (dotted line) fills a sp localized at the central region of the cylinder. Figures 2(d) and 2(e) show the z-density profile of the ND populated with $N=6$ and $N=7$ electrons. We see that in both cases four electrons are filling the spherical caps at the ND ends (we have checked that the integration of the charge density within the caps regions yield four electrons). Figures 2(d) and 2(e) also reveal that, within the cap regions, the electronic spin-up density (dotted line) equals the electronic spin-down density (dashed line), i.e., the total spin density is zero. On the other hand, the central cylinder shows full spin polarization with the spin-up density showing two (three) peaks and the spin-down profile showing a zero height. The real existence of the fully polarized phase should be taken with caution, in the sense that LSDA generally overestimates exchange and correlation in extremely diluted systems (see, e.g., Ref. 34). The same behavior takes place when removing the two ND caps, thus yielding a cylindrical NR and filling it with $N=2$ and $N=3$ electrons, [see Figs. 3(a) and 3(b)]. Furthermore, in the particular $N=6$ and $N=7$ ND cases, the total energy of the fully polarized ground state is found to be very close to the SDW state. Then, due to the above-mentioned exchange and correlation overestimation of LSDA in diluted system, the obtained result may be just considered as a signature of attainment of the extremely diluted regime. Also, it reveals the achievement of a MP in which four electrons are filling the caps forming a Fermi liquid[35] and the rest jump into the central cylinder forming a dilute phase. Another interesting feature of these two pictures, Figs. 2(d) and 2(e), is that the electrons at the cylinder are quite wavy, i.e., they behave like quantum electrons having finite extension and partially overlapping.

When an extra electron is added into the ND, in addition to the Fermi liquid in the caps at the ND ends, a nice central SDW emerges, i.e., a typical Wigner crystallization with N peaks and broken spin symmetry[19] [see Fig. 2(f)]. However, the addition energy spectrum remains flat, as corresponds to the filling of extremely diluted systems [see region after the left vertical arrow in Fig. 2(a)]. In this case, the overlap between neighbor electrons with the same spin is nearly

zero, as can be seen in Fig. 2(f), where the density profile of a given spin goes down to zero as the opposite spin-density profile reaches a maximum.

As we keep filling the ND with electrons, from $N=8$ up to $N=11$, the scenario does not change. The addition energy spectrum remains flat and the previously described MP, with Fermi liquid within the caps at the ND ends and SDW at the central cylinder, remains. However, as the number of electrons increases, they become wavier, in the sense that the overlap between neighbor electrons with the same spin starts to increase (the density profile of a given spin starts being no longer negligible at the places where the opposite spin-density profile reaches its maxima).

When the ND is filled with $N=12$ electrons, i.e., the central cylinder is populated with $N=8$ electrons, the number of maxima in the central cylinder is reduced to four, i.e., one half of the number of electrons in the trunk, as corresponds to a CDW phase. As pointed out in Sec. I, this phase arises when the density of electrons starts rising up, but it is still too low as to form a Fermi liquid. In a typical CDW, the electronic spin-up density equals the electronic spin-down one so that the corresponding profiles are superposed. However, this is not exactly the case in Fig. 2(j), which better seems a phase in between CDW and SDW. As far as the addition energy spectrum is concerned, the transition from SDW to CDW is monitorized by the end of a completely flat profile and the appearance of typical shell-filling features in the spectrum.

A typical CDW phase in the central cylinder is obtained when filling the ND with $N=14$, 16, 18, and 20 electrons [see Figs. 2(l), 2(n), 2(p), and 2(r)]. However, the odd fillings, i.e., $N=13$, 15, 17, and 19 electrons, lead to density profiles similar to that of the above-mentioned ND filled with $N=12$ electrons, where the maxima of the electronic spin-up density do not completely occur at the positions of the maxima of the electronic spin-down one so that the corresponding profiles do not completely match [see Figs. 2(k), 2(m), 2(o), and 2(q)].

This intriguing feature characteristic of the low diluted, odd-populated ND is also reproduced in the low diluted odd-populated NRs. It can be seen in Fig. 3, where the ground state z-density profiles of a NR built of a cylinder of $R=2$ nm radius, $L=55$ nm length, and populated with 3 up to 16 electrons, respectively, are displayed. This asymmetry between the spin-up and -down density profiles may come from the different self-consistent potentials appearing in the spin-up and spin-down KS equations.

Since the MPs seem to come from inhomogeneous confining potentials, we explore next the possibility of producing MPs by means of the application of an external electric field. To this end, we apply an external electric field along the z axis of the above mentioned $R=2$ nm radius and $L=55$ nm length NR. Several electric field intensities and NR populations are considered. As expected, the neat separations of the two phases found when inhomogeneity comes in the confining potential so that steplike potentials act upon the system cannot be seen when applying an electric field. As an example, we show in Fig. 4 the ground-state z-density profiles of a NR populated with $N=6$ electrons and subject to a 20 kV/cm electric field along the z axis. Three different

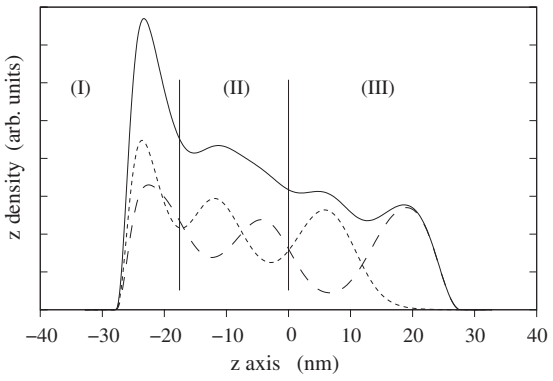

FIG. 4. NR ground state z-density profiles (the NR is modeled by a cylinder of $R=2$ nm radius and $L=55$ nm length) populated with $N=6$ electrons, subject to a 20 kV/cm electric field along the z direction. Solid line: total charge density. Dotted/dashed line: spin up/down density.

regions, labeled (I), (II), and (III) in the figure, can be distinguished in this profile. While region (III) looks like a typical SDW (Wigner crystallization) with as many peaks as electrons and broken spin symmetry, region (I) looks like a CDW with a number of peaks half the number of electrons. Finally, region (II) displays an intermediate feature. On the one hand, we can see broken spin symmetry with the maximum of the spin-up(-down) density arising at the position of the minimum of the spin-down(-up) density. On the other hand, the number of peaks is half the number of electrons.

We conclude that the presence of inhomogeneity may lead to the formation of MPs, and that structural inhomogeneities, i.e., steplike potentials coming from spatial confinement, yield the more neat MPs.

Next we explore the infrared response. Our system feels a strong radial confinement and thus the responses in the directions perpendicular to the symmetry axis of the nanostructure (transverse response), both to spin- and charge-density oscillations, arise in the high-energy region so that no peaks are found in the low-energy region of the spectrum. We enclose in Fig. 5 the transverse spin- and charge-density responses of the studied ND populated with $N=4$ [no electrons in the central cylinder, see Fig. 2(b)], $N=8$ [four electrons yielding a SDW in the central cylinder, see Fig. 2(f)], and $N=16$ [12 electrons yielding a CDW in the central cylinder, see Fig. 2(n)]. Also, the transverse spin- and charge-density responses of the NR populated with $N=4$ [yielding a SDW, see Fig. 3(c)] and $N=12$ [yielding a CDW, see Fig. 3(k)] are also enclosed in the figure for the sake of comparison.

Figure 5 reveals that the spin responses of all studied NDs have a strong peak at 450 meV which is absent in the NRs. We may associate this peak to transverse oscillations of the electrons in the ND caps. The NDs with more than four electrons show a second strong spin peak at higher energies (474 meV for $N=16$ and 483 meV for $N=8$, the latter displaying a second weaker transition at an energy a bit higher than 485 meV, see Fig. 5). Also the partner NRs (those populated with $N=4$ and $N=12$) show this strong spin peak, and it also happens that the more diluted system shows the response at a higher energy and has a second weaker transition at a bit higher energy (482 meV for $N=12$ and 492 and 494

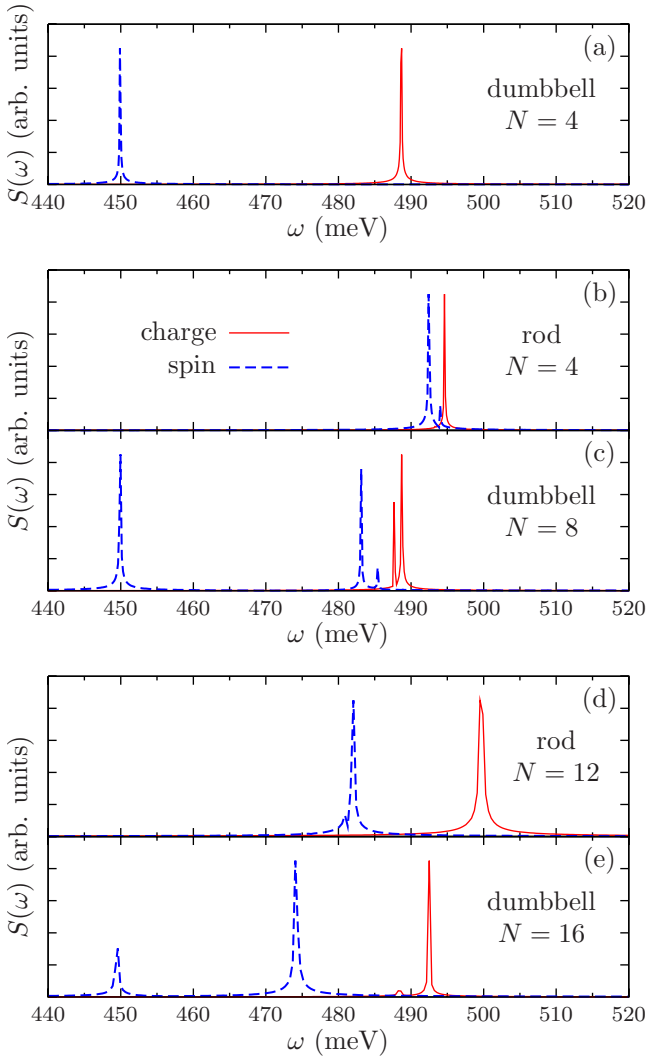

FIG. 5. (Color online) Spin-density (dashed lines) and charge-density (solid lines) transverse responses (arb. units) of different NRs and NDs. Geometry and electron population are indicated at each of the panels. Panels (b) and (c), on the one hand, and (d) and (e), on the other hand, correspond to the same number of electrons in the central cylinder (4 and 12, respectively).

meV for $N=4$). We may associate this peak to transverse-spin oscillations of the electrons in the ND cylinder and in the NR, respectively. The charge-density response arises between 487 and 500 meV, being distributed among one or two peaks for all five cases studied. Therefore, we conclude that, as expected, the transverse-spin and -charge responses do not show any fingerprint of dilute (Wigner) electronic distributions. In fact, the transitions associated to the cylinder appear at energies higher than those related to the cap, as the cylinder radius is smaller than that of the caps, thus just revealing a higher (radial) confinement.

Let us consider next the longitudinal or axial response. Figure 6 collects the low [Figs. 6(a)–6(e)] and high [Figs. 6(f)–6(j)] energy parts of the spin- and charge-density responses for the different NDs and NRs studied. As far as the high-energy part of the response concerns, we can see that for all studied ND populations the spectra have a series of regularly spaced peaks within the 160–800 meV range with a smooth envelope, the spacing between consecutive peaks slightly increasing with energy [see Figs. 6(f), 6(h), and 6(j)]. For the $N=4$ ND these peaks take all the strength for both spin- and charge-density responses [see Fig. 6(f)]. For the other two studied NDs, with $N=8,16$, the strengths of these high-energy peaks are one or more orders of magnitude smaller than those of the peaks arising at low energies—that we are going to describe next [see Figs. 6(h) and 6(j), respectively]. These peaks, absent in NRs [see Figs. 6(g) and 6(i)], can therefore be associated with the confinement in the ND caps.

Finally, we turn our attention toward the low-energy range of the longitudinal response. On the one hand, we can see in Figs. 6(e) and 6(d) that both the $N=16$ electron ND and the $N=12$ electron NR concentrate almost all the strength of their charge-density response in respective single peaks at approximately 21 meV. The same happens to their spin-density response, appearing respective single peaks between 7 and 8 meV. On the other hand, the spin response of the $N=8$ electron ND and its corresponding $N=4$ electron NR partner [see Figs. 6(c) and 6(b), respectively] arise quite fragmented in this low-energy part of the spectra. Furthermore, and in contrast with the other cases, the spin peaks appear at energies higher than those of the charge-density peaks. It is remarkable the close similarity in the response (fingerprint) of the $N=16$ ND and its $N=12$ NR partner, on the one hand, and that of the $N=8$ ND and its $N=4$ NR partner, on the other hand. Finally, the $N=4$ ND has not a single peak in this low-energy region of the spin- and charge-density responses [see Fig. 6(a)].

In general, the charge-density response emerges at energies higher than those of the spin-density response, due to the fact that the Coulomb repulsion exceeds the attraction associated with the spin and coming from the exchange-correlation term in the KS Hamiltonian. The observed feature in the systems with Wigner localization ($N=8$ ND and $N=4$ NR) seems to come from the fact that the maxima of the densities of both spins lie apart from each other forming the Wigner molecules. All the same, these spin peaks arising at energies higher than those of the charge-density might not correspond to a genuine spin response, due to the relevant local magnetization of the system, and may correspond to the so-called acoustic modes.[36]

In summary, we do have some elements allowing (i) to distinguish NDs from NRs in the transverse-spin response, (ii) to discriminate whether ND electrons are exclusively located in the caps or also in the central trunk (longitudinal high-energy response and presence or absence of peaks in its low-energy range), and finally (iii) to detect the Wigner phase in the ND trunk or in the NR: spectra fragmentation and absence of spin response at energies lower than those of the charge-density one (acoustic modes).

IV. CONCLUDING REMARKS

In the present paper we have shown that inhomogeneous confining potentials may lead to the formation of mixed phases, driven by an uneven electronic-density distribution,

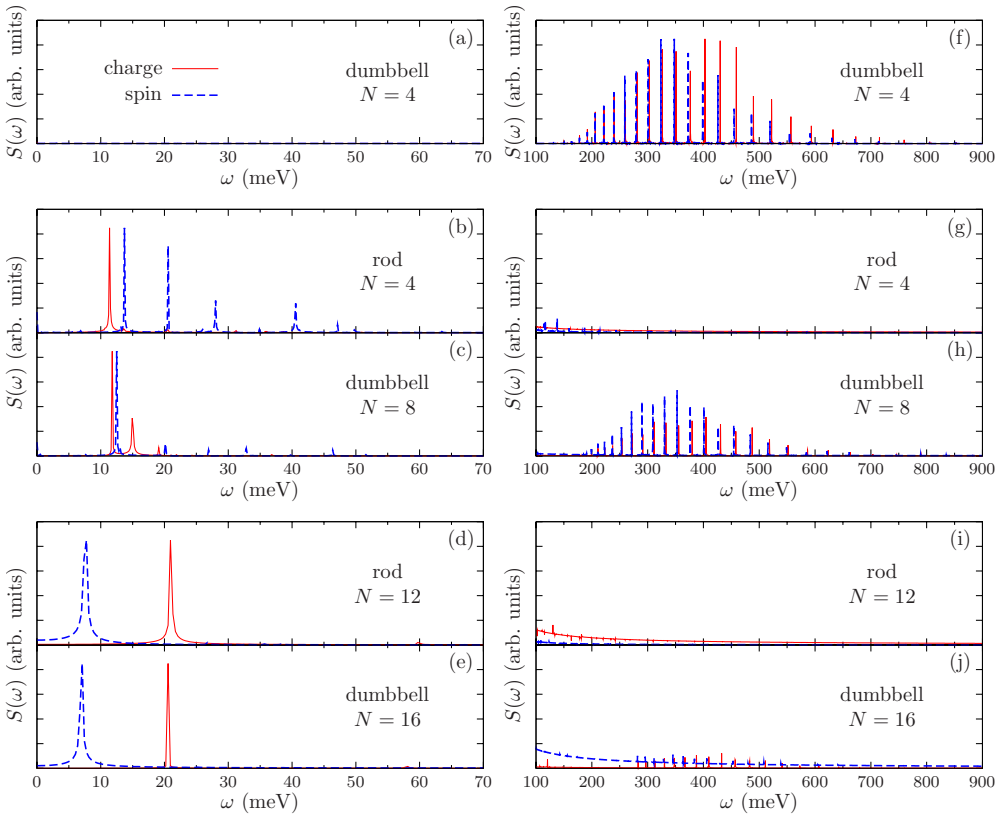

FIG. 6. (Color online) Low-energy (left column) and high-energy (right column) spin-density (dashed lines) and charge-density (solid lines) axial responses (arb. units) of different NRs and NDs. Geometry and electron population are indicated at each of the panels and both are the same for every row of panels. Grouped panels correspond to the same number of electrons in the central cylinder. Responses are magnified two orders of magnitude in panels (g)–(j) with respect to their corresponding low-energy responses in panels (b)–(e).

in which some regions of the N-electron system behave like a Fermi liquid while, simultaneously, other more dilute regions display the typical quasiclassical Wigner distribution of the charge maxima in the electron-density profile, either CDW or proper SDW. Furthermore, we have shown the characterization of MPs in the addition spectrum and the infrared response. Finally, we would like to stress that beyond its intrinsic theoretical interest, MPs may be useful in the design of optoelectronic devices. For example, the low-energy axial infrared response of a ND attached to a gate, the voltage of which is changing to fill the ND with electrons, may be used as an infrared sensor of electron filling, since once the caps are full of electrons and the next one jumps into the trunk, an abrupt low-energy infrared sign is emitted.

ACKNOWLEDGMENTS

Continuous support from MCINN under Projects No. CTQ2008-03344 and No. FIS2008-00421, UJI-Bancaixa under Project No. P1-1A2009-03, and Generalitat de Catalunya under Project No. 2009SGR1289 are gratefully acknowledged. A.B. and J.M.E. acknowledge the support from the Spanish FPI (MCINN), FPU (ME) programs, respectively.

*josep.planelles@qfa.uji.es

[1] E. P. Wigner, Phys. Rev. **46**, 1002 (1934).
[2] S. M. Reimann and M. Manninen, Rev. Mod. Phys. **74**, 1283 (2002).
[3] C. Yannouleas and U. Landman, Rep. Prog. Phys. **70**, 2067 (2007).
[4] J. P. Nikkarila and M. Manninen, Solid State Commun. **141**, 209 (2007).
[5] P. A. Maksym, Phys. Rev. B **53**, 10871 (1996).
[6] S. Weiss, M. Thorwart, and R. Egger, Europhys. Lett. **76**, 905 (2006).
[7] A. V. Filinov, M. Bonitz, and Yu. E. Lozovik, Phys. Rev. Lett. **86**, 3851 (2001).
[8] M. Bonitz, P. Ludwig, H. Baumgartner, C. Henning, A. Filinov, D. Block, O. Arp, A. Piel, S. Kading, Y. Ivanov, A. Melzer, H. Fehske, and V. Filinov, Phys. Plasmas **15**, 055704 (2008).
[9] S. M. Reimann, M. Koskinen, M. Manninen, and B. R. Mottelson, Phys. Rev. Lett. **83**, 3270 (1999).
[10] Z. A. Németh and J.-L. Pichard, Europhys. Lett. **58**, 744 (2002).
[11] M. Koskinen, M. Manninen, and S. M. Reimann, Phys. Rev.

Lett. **79**, 1389 (1997).
[12] E. Räsänen, H. Saarikoski, V. N. Stavrou, A. Harju, M. J. Puska, and R. M. Nieminen, Phys. Rev. B **67**, 235307 (2003).
[13] J. Planelles, M. Royo, A. Ballester, and M. Pi, Phys. Rev. B **80**, 045324 (2009).
[14] B. Szafran, F. M. Peeters, S. Bednarek, T. Chwiej, and J. Adamowski, Phys. Rev. B **70**, 035401 (2004).
[15] E. J. Mueller, Phys. Rev. B **72**, 075322 (2005).
[16] J. L. Movilla, J. Planelles, and W. Jaskolski, Phys. Rev. B **73**, 035305 (2006).
[17] X. Wan and R. N. Bhatt, Phys. Rev. B **65**, 233209 (2002).
[18] N. B. Zhitenev, M. Brodsky, R. C. Ashoori, L. N. Pfeiffer, and K. W. West, Science **285**, 715 (1999).
[19] The spin-symmetry breaking observed in LSDFT is not found in CI calculations (Ref. 14). An internal-space spin order appears instead so that this phase can be identified as the tendency of mean field to mimic such an internal ordering.
[20] X. Peng, L. Manna, W. Yang, J. Wickham, E. Scher, A. Kadavanich, and A. P. Alivisatos, Nature (London) **404**, 59 (2000); S. Kan, T. Mokari, E. Rothenberg, and U. Banin, Nature Mater. **2**, 155 (2003).
[21] L. Carbone, S. Kudera, C. Giannini, G. Ciccarella, R. Cingolani, P. D. Cozzoli, and L. Manna, J. Mater. Chem. **16**, 3952 (2006).
[22] F. Shieh, A. E. Saunders, and B. A. Korgel, J. Phys. Chem. B **109**, 8538 (2005).
[23] J. E. Halpert, V. J. Porter, J. P. Zimmer, and M. G. Bawendi, J. Am. Chem. Soc. **128**, 12590 (2006).
[24] M. Pi, A. Emperador, M. Barranco, and F. Garcias, Phys. Rev. B **63**, 115316 (2001).
[25] M. Pi, A. Emperador, M. Barranco, F. Garcias, K. Muraki, S. Tarucha, and D. G. Austing, Phys. Rev. Lett. **87**, 066801 (2001).
[26] A. Wensauer, O. Steffens, M. Suhrke, and U. Rössler, Phys. Rev. B **62**, 2605 (2000).
[27] J. P. Perdew and A. Zunger, Phys. Rev. B **23**, 5048 (1981).
[28] M. Pi, F. Ancilotto, E. Lipparini, and R. Mayol, Physica E **24**, 297 (2004).
[29] A. Puente and Ll. Serra, Phys. Rev. Lett. **83**, 3266 (1999).
[30] Since no specific NR (ND) environment is determined, possible polarization effects coming from the dielectric mismatch between the NR (ND) and the surrounding medium are disregarded.
[31] Ch. H. Wang, T. T. Chen, Y. F. Chen, M. L. Ho, Ch. W. Lai, and P. T. Chou, Nanotechnology **19**, 115702 (2008).
[32] J. Kainz, S. A. Mikhailov, A. Wensauer, and U. Rössler, Phys. Rev. B **65**, 115305 (2002).
[33] M. Pi, D. G. Austing, R. Mayol, K. Muraki, S. Sasaki, H. Tamura, and S. Tarucha, in *Trends in Quantum Dots Research*, edited by P. A. Ling (Nova Science, New York, 2005); D. G. Austing, S. Sasaki, K. Muraki, Y. Tokura, K. Ono, S. Tarucha, M. Barranco, A. Emperador, M. Pi, and F. Garcias, in *Nano-Physics & Bio-Electronics: A New Odyssey*, edited by T. Chakraborty, F. Peeters, and U. Sivan (Elsevier, New York, 2002).
[34] F. Pederiva, A. Emperador, and E. Lipparini, Phys. Rev. B **66**, 165314 (2002).
[35] Since only two electrons fill a cap, one cannot actually distinguish a Fermi liquid from a CDW. In both cases only a peak arises in the density profile. However, we have checked that when the same electronic density is obtained by filling with four electrons a (larger) spherical QD a Fermi liquid results.
[36] O. Mayrock, S. A. Mikhailov, T. Darnhofer, and U. Rössler, Phys. Rev. B **56**, 15760 (1997); O. Mayrock, S. A. Mikhailov, O. Steffens, and U. Rössler, Physica E **1**, 232 (1998).